VSC-HVDC Transmission Line Protection Based on Dynamic State Estimation

Binglin Wang[1], *Student Member, IEEE*, Yu Liu[1,2,*], *Member, IEEE*
1. School of Information Science and Technology, ShanghaiTech University, Shanghai, China, 201210
2. Key Laboratory of Control of Power Transmission and Conversion (SJTU), Ministry of Education, Shanghai, 200240
*Email: liuyu@shanghaitech.edu.cn

Abstract: Voltage Source Converter based High Voltage Direct Current (VSC-HVDC) transmission line protection is of significance for the safe and stable operation of VSC-HVDC systems. In this paper, a dynamic state estimation (DSE) based VSC-HVDC line protection method is proposed. The method is an extension of the current differential protection, considers the distributed shunt capacitance through the line and can be used as the line primary protection. Specifically, the dynamic model that describes all physical laws that the VSC-HVDC line under protection should obey is first established. Afterwards, the consistency between available measurements and the dynamic model is determined by DSE and the line is tripped if the consistency is continuously low for a user-defined period of time. Numerical experiments demonstrate its dependable and fast operation during internal faults, secure refusal of operation during external faults, sensitivity for high impedance faults and robustness towards measurement noises.

Key words: VSC-HVDC transmission line protection, dynamic state estimation, high impedance faults, measurement noise

I. INTRODUCTION

VOLTAGE Source Converter based High Voltage Direct Current (VSC-HVDC) systems are widely applied in practical DC transmission systems [1]. Compared to traditional Line Commutated Converter based High Voltage Direct Current (LCC-HVDC) systems, VSC-HVDC systems have the advantages such as flexible control, reliable commutation, low harmonics and no need for reactive power by AC source [2]. Nevertheless, unlike LCC-HVDC systems, the current will increase rapidly to the level of damaging power electronic devices during faults in VSC-HVDC systems [3]. One traditional way to ensure device safety during line faults is to block the two converters at terminals of the line. With the development of the high speed DC circuit breaker (DCCB), protective relaying is a better choice than blocking converters. For example, when a single pole fault occurs, power can be transported through another pole as long as the faulted line is isolated [4], to minimize the power outage range. Therefore, the protection of the transmission line is of great significance to guarantee the safe and stable operation of the VSC-HVDC systems.

Existing VSC-HVDC transmission line protection methods can be classified into primary protection functions and backup protection functions. The primary protection offers immediate response to the fault in the protection zone. The backup protection should operate in case of failures of the primary protection.

This work is sponsored by National Nature Science Foundation of China (No. 51807119), Shanghai Pujiang Program (No. 18PJ1408100) and Key Laboratory of Control of Power Transmission and Conversion (SJTU), Ministry of Education (No. 2015AB04). Their support is greatly appreciated.

Primary protection functions of VSC-HVDC transmission lines can be further categorized into single-ended and dual-ended protection functions. **Single ended primary protection functions** utilize local measurements and do not require communication channels, such as travelling wave protection and voltage derivative protection [5]. Traveling wave distance protection methods borrow the idea of distance protection in AC transmission lines. These methods determine the distance between the local terminal and the fault by the time difference of the subsequent arrival of travelling waves at the local terminal [6]. However, the main limitation is that the method cannot protect the entire line instantaneously due to selectivity issue. To ensure selectivity of the protection algorithm, researchers proposed boundary protection algorithms [7] that utilize the attenuation characteristics of the boundary devices such as smoothing reactors. The current transient caused by external faults, especially with high frequency, will be attenuated through the smoothing reactor. However, the effectiveness of the protection criterion depends on the existence of boundary devices. **Dual ended primary protection functions** utilize measurements from both terminals of the line. A proper communication channel is usually required to exchange information between terminals of the line. Most of dual ended methods are based on characteristics of traveling waves generated by the fault. For example, the dual ended traveling wave directional comparison pilot protection method [8] calculates the direction of fault current component to distinguish the fault direction; the traveling wave pilot distance protection method [9] compares the results of traveling wave distance functions at both terminals to distinguish internal/external faults. Nevertheless, traveling wave based protection schemes are usually based on the reliable detection of the initial travelling wave, which could be problematic especially during high impedance faults or faults that caused by gradual change of transition resistance.

Backup protection functions of VSC-HVDC can also be further classified into single-ended and dual-ended protection functions. **Single ended backup protection functions** include DC under-voltage protection and DC over-voltage protection. These functions simply trip the line if the deviation of the terminal voltage from the rated voltage exceeds a threshold for a user-defined period of time with detecting a high rate of voltage changing at beginning [10]. However, these methods in principle cannot differentiate between internal and external faults, making hard to provide the settings of these protection methods. The most widely used **dual ended backup protection function** is the current differential protection. The main idea is to monitor whether the sum of instantaneous

978-1-7281-1981-6/19/$31.00 ©2019 IEEE

terminal currents is zero [11]. However, the method is largely affected by the capacitive charging currents especially during system disturbances [12] and therefore the method is usually deployed with a long time delay [13].

Current differential protection is actually a very effective primary protection function in existing AC transmission lines [12] and potentially a good candidate for the VSC-HVDC transmission line protection. However, in VSC-HVDC systems, the shunt capacitive currents in transmission lines are extremely large especially during system transients such as external faults. To avoid mal-operation during severe external faults, the settings (thresholds and delays) of the current differential protection in VSC-HVDC transmission lines have to be extremely conservative, making it not applicable for the primary protection of VSC-HVDC transmission lines. To overcome this problem, this paper proposes a primary VSC-HVDC line protection method based on Dynamic State Estimation (DSE), which is an extension of the current differential protection [12]. Instead of only validating Kirchhoff's Current Law (KCL) as in current differential protection, the proposed method constructs the protection algorithm by validating all physical laws that the VSC-HVDC line should obey, including KCL, Kirchhoff's Voltage Law (KVL), etc. In this case, the shunt capacitance can be fully considered in this proposed method.

Specifically, the proposed DSE based protection method monitors the consistency between the available measurements and the dynamic model that describes physical laws of a healthy VSC-HVDC line (without internal fault). This consistency should be high during normal operation or external faults, while it should be low during internal faults. This difference is the key to identify internal faults. Due to space limitations, this paper will only show the performance of the algorithm on two-terminal VSC-HVDC lines, however, this proposed protection method can be similarly applied to multi-terminal VSC-HVDC transmission lines. The rest of the paper is arranged as follows. Section II introduces the VSC-HVDC transmission line dynamic model. Section III proposes the DSE based protection algorithm. Section IV demonstrates the numerical results of the proposed protection method. Section V draws a conclusion.

II. VSC-HVDC Transmission Line Dynamic Model

This DSE based protection method requires a highly fidelity dynamic model of VSC-HVDC transmission line. In this chapter, the dynamic model with the form of algebraic and differential equations is first developed. Afterwards, the dynamic model described with algebraic and differential equations is equivalently transformed into the dynamic model with only algebraic equations using the quadratic integration method.

A. Algebraic and differential form of the dynamic model

The transmission line dynamic model is described mathematically by a set of differential equations, which contains physical laws that a healthy VSC-HVDC transmission line should obey. To fully consider distributed capacitance through the whole line, a multi- section line model is utilized, where each section is a π equivalent line model for short lines. To ensure the accuracy of the line model, the section number is selected in such a way that the traveling length of the electromagnetic wave during one sampling interval is comparable to the length of each section.

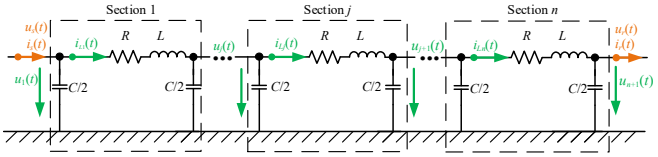

Figure 1. Transmission line model under protection

Figure 1 shows an example transmission line model with n sections. Node voltage $u_j(t),(j=1,2,\cdots,n+1)$ and current flowing through each section $i_{Lj}(t),(j=1,2,\cdots,n)$ are considered as states. Currents $i_s(t)$ and $i_r(t)$, voltages $u_s(t)$ and $u_r(t)$ at both terminals are considered as actual measurements. There are also some virtual voltage and current measurements (0 measurement values) that describes the relationship among states. The algebraic and differential form of the dynamic model is,

$$\begin{aligned}
&i_s(t)=i_{L1}(t)+C/2\cdot du_1(t)/dt\\
&i_r(t)=i_{Ln}(t)-C/2\cdot du_{n+1}(t)/dt\\
&\vdots\\
&0=-i_{Lj}(t)+i_{L(j+1)}(t)+C\cdot du_{j+1}(t)/dt\ (j=1,2,,n-1)\\
&\vdots\\
&0=-u_j(t)+u_{j+1}(t)+Ri_{Lj}+L\cdot di_{L1}/dt\ (j=1,2,,n)\\
&\vdots\\
&u_s(t)=u_1(t),u_r(t)=u_{n+1}(t)
\end{aligned} \tag{1}$$

Rewrite equation (1) in matrix form,

$$\begin{cases}
\boldsymbol{i}(t)=\boldsymbol{A}_1\cdot\boldsymbol{x}(t)+\boldsymbol{B}_1\cdot d\boldsymbol{x}(t)/dt\\
\boldsymbol{0}_{2n-1}=\boldsymbol{A}_2\cdot\boldsymbol{x}(t)+\boldsymbol{B}_2\cdot d\boldsymbol{x}(t)/dt\\
\boldsymbol{u}(t)=\boldsymbol{A}_3\cdot\boldsymbol{x}(t)+\boldsymbol{B}_3\cdot d\boldsymbol{x}(t)/dt
\end{cases} \tag{2}$$

where the current measurement vector is $\boldsymbol{i}(t)=\left[i_s(t)\quad i_r(t)\right]^T$, voltage measurement vector is $\boldsymbol{u}(t)=\left[u_1(t)\quad u_{n+1}(t)\right]^T$, the state vector is $\boldsymbol{x}(t)=\left[u_1(t)\ \cdots\ u_{n+1}(t)\quad i_{L1}(t)\ \cdots\ i_{Ln}(t)\right]^T$, $\boldsymbol{A}_j$ and $\boldsymbol{B}_j\ (j=1,2,3)$ are corresponding coefficient matrices.

B. Algebraic form of the dynamic model

To solve the states of the model in equation (2), the dynamic model in algebraic and differential form can be transformed into the dynamic model in pure algebraic form. In order to achieve this step, the quadratic integration method [14] is utilized. Equation (2) is integrated over two different time intervals $[t-h\quad t]$ and $[t-h\quad t_m]$ respectively, where h equals twice sampling step and $t_m=t-h/2$. Algebraic form of the dynamic model is,

$$\boldsymbol{z}(t,t_m)=\boldsymbol{Y}_{eqx}\cdot\boldsymbol{x}(t,t_m)-\boldsymbol{B}_{eq} \tag{3}$$

where $\boldsymbol{z}(t,t_m)=\left[\boldsymbol{i}(t)\quad\boldsymbol{0}_{2n-1}\quad\boldsymbol{i}(t_m)\quad\boldsymbol{0}_{2n-1}\quad\boldsymbol{u}(t)\quad\boldsymbol{u}(t_m)\right]^T$, $\boldsymbol{x}(t,t_m)=\left[\boldsymbol{x}(t)\quad\boldsymbol{x}(t_m)\right]^T$, $\boldsymbol{B}_{eq}=-\boldsymbol{N}_{eqx}\boldsymbol{x}(t-h)-\boldsymbol{M}_{eq}\boldsymbol{i}(t-h)$, and

$$\boldsymbol{M}_{eq}=\begin{bmatrix}\boldsymbol{I}_{size(i(t))} & \boldsymbol{0}_{(2n-1)\times(2n+1)} & -\boldsymbol{I}_{size(i(t))}/2 & \boldsymbol{0}_{(2n-1)\times(2n+1)} & \boldsymbol{0}_{2\times(2n+1)} & \boldsymbol{0}_{2\times(2n+1)}\end{bmatrix}^T$$

$$\boldsymbol{Y}_{eqx}=\begin{bmatrix}\boldsymbol{A}_1+4\boldsymbol{B}_1/h & -8\boldsymbol{B}_1/h\\ \boldsymbol{A}_2+4\boldsymbol{B}_2/h & -8\boldsymbol{B}_2/h\\ \boldsymbol{B}_1/(2h) & \boldsymbol{A}_1+2\boldsymbol{B}_1/h\\ \boldsymbol{B}_2/(2h) & \boldsymbol{A}_2+2\boldsymbol{B}_2/h\\ \boldsymbol{A}_3 & \boldsymbol{0}_{2\times(2n+1)}\\ \boldsymbol{0}_{2\times(2n+1)} & \boldsymbol{A}_3\end{bmatrix},\ \boldsymbol{N}_{eqx}=\begin{bmatrix}-\boldsymbol{A}_1+4\boldsymbol{B}_1/h\\ -\boldsymbol{A}_2+4\boldsymbol{B}_2/h\\ \boldsymbol{A}_1/2-5\boldsymbol{B}_1/(2h)\\ \boldsymbol{A}_2/2-5\boldsymbol{B}_2/(2h)\\ \boldsymbol{0}_{2\times(2n+1)}\\ \boldsymbol{0}_{2\times(2n+1)}\end{bmatrix}$$

III. DSE STATE ESTIMATION BASED PROTECTION METHOD

According to the algebraic form of the dynamic model, DSE is used to obtain the best estimation of the state vector $\hat{\boldsymbol{x}}(t,t_m)$. Afterwards, the consistency between measurements and the dynamic model is quantified. In each step of DSE, the measurements at two sampling time (t and t_m) are available. With known measurements and states at time $t-h$.

A. WLS Dynamic State Estimation

One way of DSE is to use the Weighted Least Square (WLS) approach. The problem of solving equation (3) is converted to an optimization problem that minimizes the weighted sum of residual squares,

$$\min_{\boldsymbol{x}(t,t_m)} J(\boldsymbol{x})=\boldsymbol{r}(t,t_m)^T\boldsymbol{W}\boldsymbol{r}(t,t_m) \tag{4}$$

where the residual is defined as the difference between the estimated measurements and actual measurements,

$$\boldsymbol{r}(t,t_m)=\boldsymbol{Y}_{eqx}\boldsymbol{x}(t,t_m)-\boldsymbol{B}_{eq}-\boldsymbol{z}(t,t_m) \tag{5}$$

The best estimation of the state vector $\hat{\boldsymbol{x}}(t,t_m)$ is,

$$\hat{\boldsymbol{x}}(t,t_m)=\left(\boldsymbol{Y}_{eqx}^T\boldsymbol{W}\boldsymbol{Y}_{eqx}\right)^{-1}\boldsymbol{Y}_{eqx}^T\boldsymbol{W}\left(\boldsymbol{z}(t,t_m)+\boldsymbol{B}_{eq}\right) \tag{6}$$

where $\boldsymbol{W}=\mathrm{diag}\left\{1/\sigma_1^2,1/\sigma_2^2,\cdots\right\}$ and σ_i is the standard deviation of the i^{th} measurement in $\boldsymbol{z}(t,t_m)$.

B. Quantification of the consistency

After obtaining the best estimation of the state vector $\hat{\boldsymbol{x}}(t,t_m)$, the corresponding residual vector $\hat{\boldsymbol{r}}(t,t_m)$ and the weighted sum of residual squares $\hat{J}(t)$ can be updated by substituting $\boldsymbol{x}(t,t_m)=\hat{\boldsymbol{x}}(t,t_m)$ into equation (4) and (5).

Note that $\hat{J}(t)$ represents the consistency between the measurements and the dynamic model. If the line is in healthy condition and the measurement errors satisfy the Gaussian distribution, $\hat{J}(t)$ satisfies the chi-square distribution [15] ($\hat{J}(t)$ is also known as the chi-square value). This implies that $\hat{J}(t)$ is likely to be a small value if the line is in healthy condition (the consistency between the measurements and the dynamic model is high). On the contrary, if the value of $\hat{J}(t)$ is large (beyond the range of chi-square distribution), the consistency between the measurements and the dynamic model is low and this is due to internal faults that changes the dynamic model of the line. The consistency is quantified with the following binary variable,

$$test(t)=\begin{cases}1, & \hat{J}(t)\ge J_{set}\\ 0, & \hat{J}(t)<J_{set}\end{cases} \tag{7}$$

where J_{set} is the threshold setting; $test(t)=0$ means that the measurements fit the model well and the line under protection is healthy (high consistency), while $test(t)=1$ indicates a possible internal fault (low consistency).

C. Criterion of the protection

To ensure security of the protection algorithm especially during system transients, the trip signal is issued if $trip(t)$ defined in equation (8) is equal to 1, i.e. if $test(t)$ keeps 1 for a user defined period of time T_{set}.

$$trip(t)=\begin{cases}1, & \int_{t-T_{set}}^{t}test(\tau)d\tau=T_{set}\\ 0, & \int_{t-T_{set}}^{t}test(\tau)d\tau<T_{set}\end{cases} \tag{8}$$

IV. SIMULATION RESULTS

An example VSC-HVDC bipolar transmission system is shown in Figure 2. The length of the transmission line is 300km. The rated voltage and the rated capacity of this bipolar transmission system are ±500kV and 2000MVA, respectively. The line under protection is the positive pole of the system, i.e. S1-R1, which is a 500kV, 1000MVA, 300km transmission line. The voltage and current instantaneous measurements are installed at both terminals of the line ($U_s(t)$, $U_r(t)$, $I_s(t)$ and $I_r(t)$ are shown in the Figure 2), with sampling rate 20 kilo-samples per second. In this simulation model, the transmission line is modeled as a multi-section model where each section is a π-equivalent model. The section number is selected as 20, which is a very good approximation of a fully distributed parameter transmission line mode.

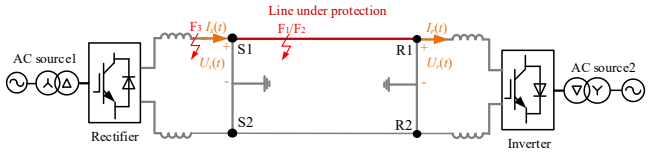

Figure 2. VSC-HVDC transmission system with faults

In order to verify the protection performance of this proposed method, considerable amount of fault events are simulated. Due to space limitations, here we only demonstrate the results of following three fault events as shown in the Figure 2. They include internal low impedance fault F_1, internal high impedance fault F_2 and external low impedance severe fault F_3. In addition, to make the system more practical, noises are added to voltage and current measurements at both terminals of the line. The noise is assumed to be with Gaussian distribution with 1% p.u. standard deviation and zero mean. The settings of the proposed protection are $J_{set}=2500$ and $T_{set}=2\,ms$. Detailed performances of the proposed protection method are demonstrated as follows.

A. Fault event 1: Internal low impedance single pole to ground fault

A positive pole to ground internal fault with 0.001 Ω occurs at 90 km away from the terminal S1 and at time 1.7 s (fault F_1). The measured values, estimated values and the residuals of voltages and currents at both terminals of the line are shown in Figure 3 and 4, respectively. We can observe that before the fault, the residuals between the estimated and actual measurements are near zero. During the fault, the residuals

increase rapidly, which indicates inconsistency between the measurements and the dynamic model.

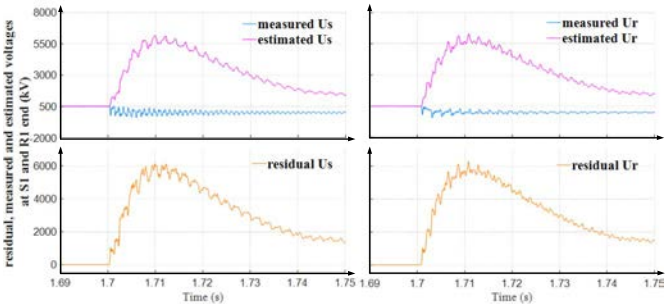

Figure 3. Voltage results: Internal fault event 1

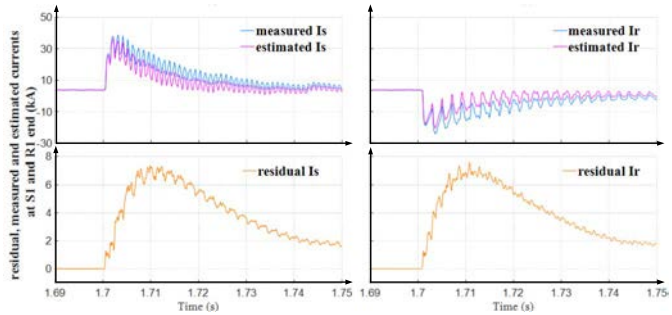

Figure 4. Current results: Internal fault event 1

To further quantify the residuals, the values of chi-square, $test(t)$ and $trip(t)$ are shown in Figure 5. The threshold $J_{set} = 2500$ is depicted in red in the first subfigure. The fault is detected at 1.7004 s when the chi-square value exceeds the threshold (only 0.4 ms after the fault occurs) and the line is tripped with 2ms delay at 1.7024 s.

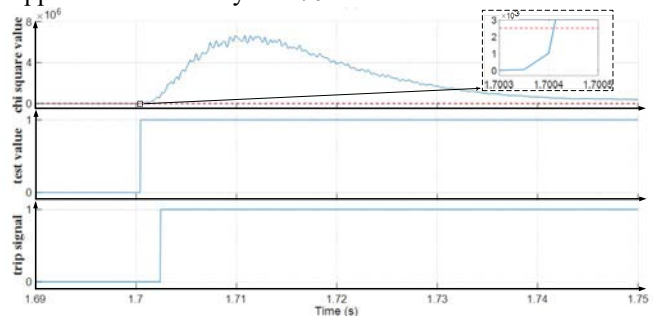

Figure 5. Protection results: Internal fault event 1

B. *Fault event 2: Internal high impedance single pole to ground fault*

A positive pole to ground internal fault with 300 Ω occurs at 90 km away from the terminal S1 and at time 1.7 s (fault F_2). The measured values, estimated values and the residuals of voltages and currents at both terminals of the line are shown in Figure 6 and 7, respectively. We can observe that before the fault, the residuals between the estimated and actual measurements are near zero. During the fault, there is still an obvious increase of residuals, which indicates inconsistency between the measurements and the dynamic model.

To further quantify the residuals, the values of chi-square, $test(t)$ and $trip(t)$ are shown in Figure 8. The threshold $J_{set} = 2500$ is depicted in red in the first subfigure. The fault is detected at 1.7033 s when the chi-square value exceeds the threshold (3.3 ms after the fault occurs for a high impedance internal fault) and the line is tripped with 2ms delay at 1.7053 s.

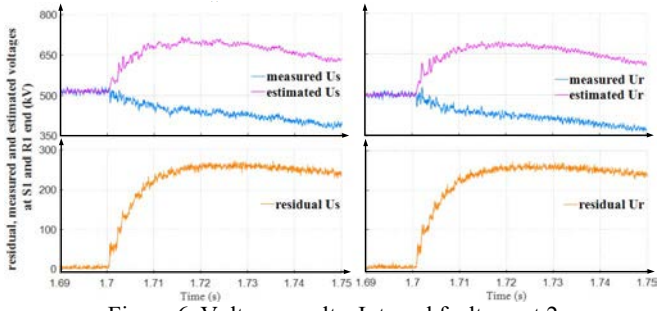

Figure 6. Voltage results: Internal fault event 2

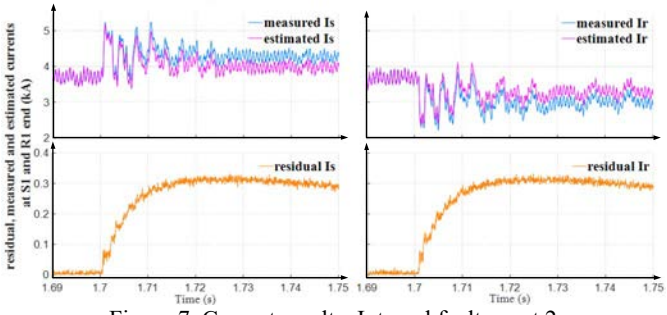

Figure 7. Current results: Internal fault event 2

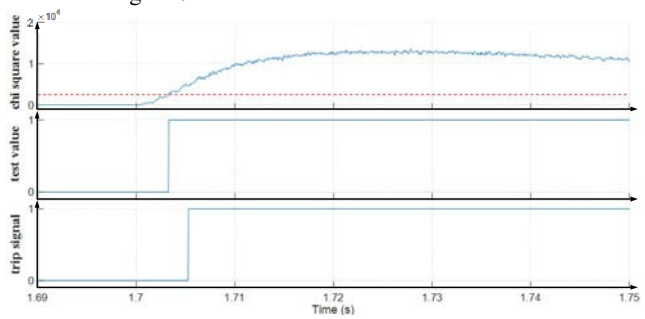

Figure 8. Protection results: Internal fault event 2

C. *Fault event 3: External low impedance single pole to ground fault*

A positive pole to ground external fault with 0.001 Ω occurs at the right terminal of the inductor and at time 1.7 s (fault F_3). Note that the fault is near the terminal S1 of the line and is a severe external fault. The measured values, estimated values and the residuals of voltages and currents at both terminals of the line are shown in Figure 9 and 10, respectively. We can observe that before the fault occurs, the residuals between the estimated and actual measurements are near zero. During the fault, the residuals first experience transients (with several peaks) and very quickly return to small values.

To further quantify the residuals, the values of chi-square, $test(t)$ and $trip(t)$ are shown in Figure 11. The threshold $J_{set} = 2500$ is depicted in red in the first subfigure. The value of $test(t)$ reaches to 1 for only two samples (0.1 ms due to system transients, which is far less than the setting 2 ms) and then remains at zero for the rest of the duration. Therefore, the protection algorithm can correctly ignore this external fault.

D. *Discussion*

From the aforementioned events, we can observe that unlike the current differential protection which requires a long delay for tripping internal faults, the proposed protection method, which is an extension of the current differential protection, can reliably trip internal faults very fast and at the same time

securely ignore external faults. These advantages of the proposed method over the traditional current differential protection are actually brought by the fact that the proposed method fully considers the distributed shunt capacitive currents through the whole length of the line.

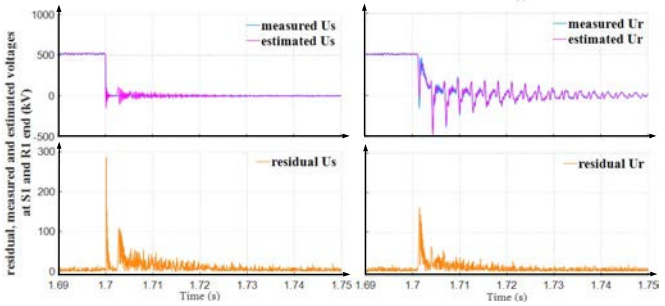

Figure 9. Voltage results: External fault event 3

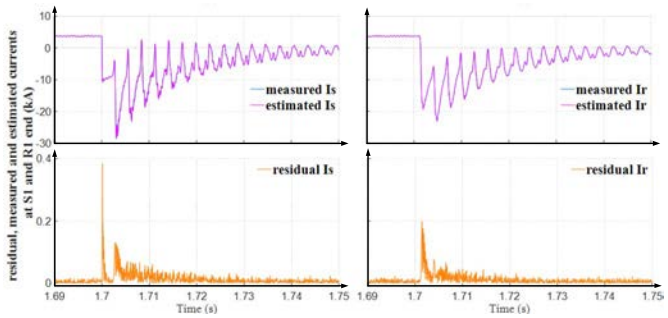

Figure 10. Current results: External fault event 3

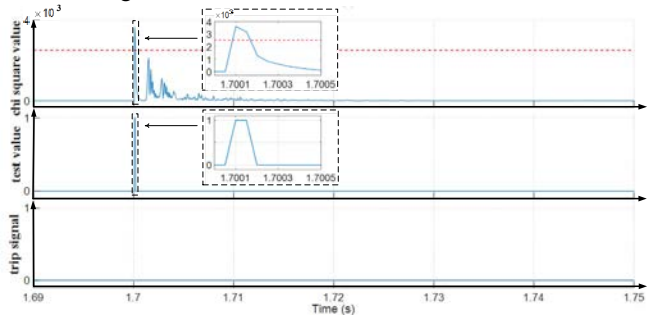

Figure 11. Protection results: External fault event 3

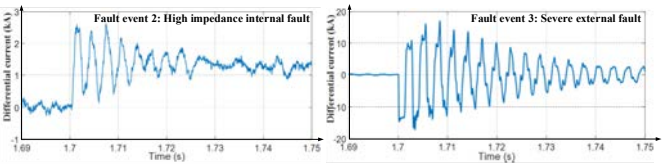

Figure 12. Differential current in the high impedance internal fault event and the severe external fault event

Figure 12 shows the differential currents (differences of instantaneous currents between two terminals) in event 2 (a high impedance internal fault) and event 3 (a severe external fault). The differential current reaches 2.5 kA during the high impedance internal fault but reaches 17 kA during the severe external fault (with long transients for external faults). Therefore, a long delay is required to ensure dependability of the current differential protection. On the other hand, from section IV.B and C, we can observe that the chi-square value during the high impedance internal fault is much larger than that during the severe external fault (with short transients for external faults). These results show a large margin to provide proper settings for the proposed protection method.

Nevertheless, the authors want to mention that the paper did not consider frequency-dependent parameters of the line. This may affect the performance of the methodology especially during system transients. Related topics will be discussed in future publications.

V. Conclusion

This paper proposes a dynamic state estimation based protection method for the VSC-HVDC transmission line. The method is an extension of the current differential protection and it considers distributed shunt capacitance through the line. The protection logic is formulated by testing the consistency between the available measurements and the accurate dynamic model of the VSC-HVDC transmission line under protection using the dynamic state estimation procedure. Numerical experiments demonstrate that the proposed method can (a) dependably detect and trip internal faults, including high impedance faults; (b) securely ignore system transients such as severe external faults; (c) reliably operate with measurement noises. Therefore, the proposed method can be used as the primary protection of the VSC-HVDC transmission line.

References

[1] N. Flourentzou, V. G. Agelidis and G. D. Demetriades, "VSC-based HVDC power transmission systems: An Overview," *IEEE Trans. Power Electron.*, vol. 24, no. 3, Mar. 2009, pp. 592-602.

[2] S. Li, W. Chen, X. Yin and D. Chen, "Protection scheme for VSC-HVDC transmission lines based on transverse differential current," *IET Gener. Transm. Distrib.*, vol. 11, no. 11, Sep. 2017, pp. 2805-2813.

[3] L. Tang, X. Dong, S. Shi and B. Wang, "Analysis of the characteristics of fault-induced travelling waves in MMC-HVDC grid," *IET J. Eng.*, vol. 2018, no. 15, Oct. 2018, pp. 1349-1353.

[4] N. Tong, X. Lin, Y. Li, Z. Hu, N. Jin, F. Wei and Z. Li, "Local measurement-based ultra-high-speed main protection for long distance VSC-MTDC," *IEEE Trans. Power Del.*, in press.

[5] Z. He, K. Liao, "Natural frequency-based protection scheme for voltage source converter-based high voltage direct current transmission lines," *IET Gener. Transm. Distrib.*, vol. 5, no. 4, Sep. 2015, pp. 1519-1525.

[6] P.A. Crossley, P.G. McLaren, "Distance protection based on travelling waves," *IEEE Trans. Power App. Syst.*, vol. PAS-102, no. 9, Sep. 1983, pp. 163-173.

[7] X. Liu, A. H. Osman, O. P. Malik, "Hybrid traveling wave/boundary protection for monopolar HVDC line," *IEEE Trans. Power Del.*, vol. 24, no. 2, Feb. 2009, pp. 569-578.

[8] Y. Wang, B. Zhang, "A novel hybrid directional comparison pilot protection scheme for the LCC-VSC hybrid HVDC transmission lines," *13th International Conference on Development in Power System Protection 2016 (DPSP)*, Edinburgh, UK, Dec. 2016, pp. 1-6.

[9] H. Seyedi, L. Behroozi. "New distance relay compensation algorithm for double-circuit transmission line protection," *IET Gener. Transm. Distrib.*, vol. 5, no. 10, Oct. 2011, pp. 1011-1018.

[10] Li, Z. Cai, Q. Sun, X. Li, D. Ren and Z. Yang, "Study on the dynamic performance characteristics of HVDC control and protections for the HVDC line fault," *IEEE Power Energy Soc. Gen. Meet., Calgary, AB, Canada*, 2009, pp. 1-5.

[11] Y. Liu, S. Meliopoulos, R. Fan, L. Sun and Z. Tan, "Dynamic state estimation based protection on series compensated transmission lines", *IEEE Trans Power Del.*, vol. 32, no. 5, Oct. 2017, pp 2199-2209.

[12] X. Zheng, N. Tai, J. S. Thorp and G. Yang, "A transient harmonic current protection scheme for HVDC transmission line," *IEEE Trans. Power Del.*, vol. 27, no. 4, Oct. 2012, pp. 2278-2285.

[13] Kong, Z. Hao, S. Zhang, and B. Zhang, "Development of a novel protection device for bipolar HVDC transmission lines," *IEEE Trans. Power Del.*, vol. 29, no. 5, Oct. 2014, pp. 2270-2278.

[14] A. P. Meliopoulos, G. J. Cokkinides, and G. K. Stefopoulos, "Quadratic integration method," *Power Syst. Transients Conf.*, Montreal, Canada, 2005.

[15] C. Schweppe and R. D. Masiello, "A tracking static state estimator," *IEEE Trans. Power App. Syst.*, vol. PAS-90, no. 3, May 1971, pp. 1025–1033.